Engineered Regeneration 4 (2023) 1–11

Contents lists available at ScienceDirect

Engineered Regeneration

journal homepage: http://www.keaipublishing.com/en/journals/engineered-regeneration/

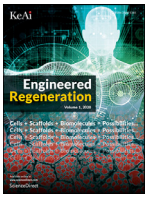

Bioactive 3D-printed chitosan-based scaffolds for personalized craniofacial bone tissue engineering

Satar Yousefiasl[a], Esmaeel Sharifi[b], Erfan Salahinejad[c], Pooyan Makvandi[d], Soussan Irani[e,*]

[a] School of Dentistry, Hamadan University of Medical Sciences, Hamadan 6517838736, Iran
[b] Department of Tissue Engineering and Biomaterials, School of Advanced Medical Sciences and Technologies, Hamadan University of Medical Sciences, Hamadan, Iran
[c] Faculty of Materials Science and Engineering, K. N. Toosi University of Technology, Tehran, Iran
[d] Centre for Materials Interfaces, Istituto Italiano di Tecnologia, viale Rinaldo Piaggio 34, Pontedera, Pisa 56025, Italy
[e] Dental Research Centre, Oral Pathology Department, Dental Faculty, Hamadan University of Medical Sciences, Hamadan, Iran

ARTICLE INFO

Keywords:
Bioactivity
CAD/CAM
Maxillofacial reconstruction
Pore
Stem cells

ABSTRACT

Regeneration of craniofacial bone defects is a key issue in the bone regeneration field. Hence, novel treatment strategies, such as tissue engineering using porous scaffolds, have been developed. An ideal tissue-engineered scaffold for bone tissue regeneration should possess pores to facilitate nutrients transmission and support reparative tissue ingrowth, bioactivity for osteoconduction and osseointegration, and biocompatibility to improve cell attachment, proliferation, and extracellular matrix formation. In the present study, we manufactured chitosan-based hydrogels substituted with alginate with optimized properties by extrusion-based three-dimensional (3D) printing. 3D printing of the scaffolds enables the designing and developing of complex architectures for craniofacial reconstruction using computer-aided design (CAD). Different ratios (2.5, 5, and 10%) of hydroxyapatite were added to the hydrogel, printed, and subsequently lyophilized to augment the physical and biological characteristics of the scaffolds. Hydroxyapatite incorporation into the chitosan-based scaffolds increased the porosity and pore size of the printed scaffolds. In addition, the presence of hydroxyapatite amplified apatite formation and decreased the size of formed apatite crystals. All the scaffold samples showed biocompatible properties and did not have toxicity toward rat bone marrow mesenchymal stem cells. Furthermore, the scaffolds containing 5% w/w hydroxyapatite exhibited significant growth in cell viability compared to the control. Overall, it is concluded that chitosan-based scaffolds adorned with hydroxyapatite are considerable for regenerating craniofacial bone defects.

1. Introduction

Bone is a dynamic connective tissue with a highly mineralized architecture, offering excellent strength and serving as a structural basis for the human body and muscles. For the proper development of the skeleton, bone undergoes dynamic modeling and remodeling processes, including the development of bone formation and resorption. There is an increasing demand for dental, craniofacial, and orthopedic regeneration and repair as the world's elderly population grows [1]. Oral and craniofacial bone lesions vary considerably from small bony defects, namely periodontal and peri-implant defects, to severe and significant defects brought on by trauma, tumor excision, and congenital deformities, affecting aesthetic appearance and functionality [2].

Autologous and allogeneic bone grafts are the most clinically applied graft treatments. Autologous bone grafting is regarded as the gold standard with acceptable clinical success. However, several limitations are associated with bone regeneration treatment methodologies of this approach, including donor site morbidity, limited availability, and surgical risks. Hence, a paucity of optimal treatment for oral and craniofacial bone tissue regeneration is still a significant challenge in dentistry, surgery, and medicine and has led to the emerging application of bone tissue engineering [3].

Bone tissue engineering combines scaffolds, cells, and biological factors to reconstruct, regenerate, and repair bone tissue. Scaffolds play a pivotal role in bone tissue engineering since they provide mechanical and structural support for cells to attach and offer a proper microenvironment that affects cell survival, proliferation, and differentiation, which leads to bone tissue formation. An ideal scaffold should display biocompatibility and controlled biodegradability in addition to suitable microarchitecture. An interconnected porous structure is essential for nutrient and oxygen uptake and waste diffusion. Pores expand the available surface area, enhancing cell migration into the scaffold and interaction with surrounding tissues [4,5]. The pore size influences cell attachment, growth, and differentiation. Furthermore, the pore size

* Corresponding author.
E-mail address: sousanirani@gmail.com (S. Irani).

https://doi.org/10.1016/j.engreg.2022.09.005
Received 2 September 2022; Received in revised form 21 September 2022; Accepted 22 September 2022
Available online 24 September 2022

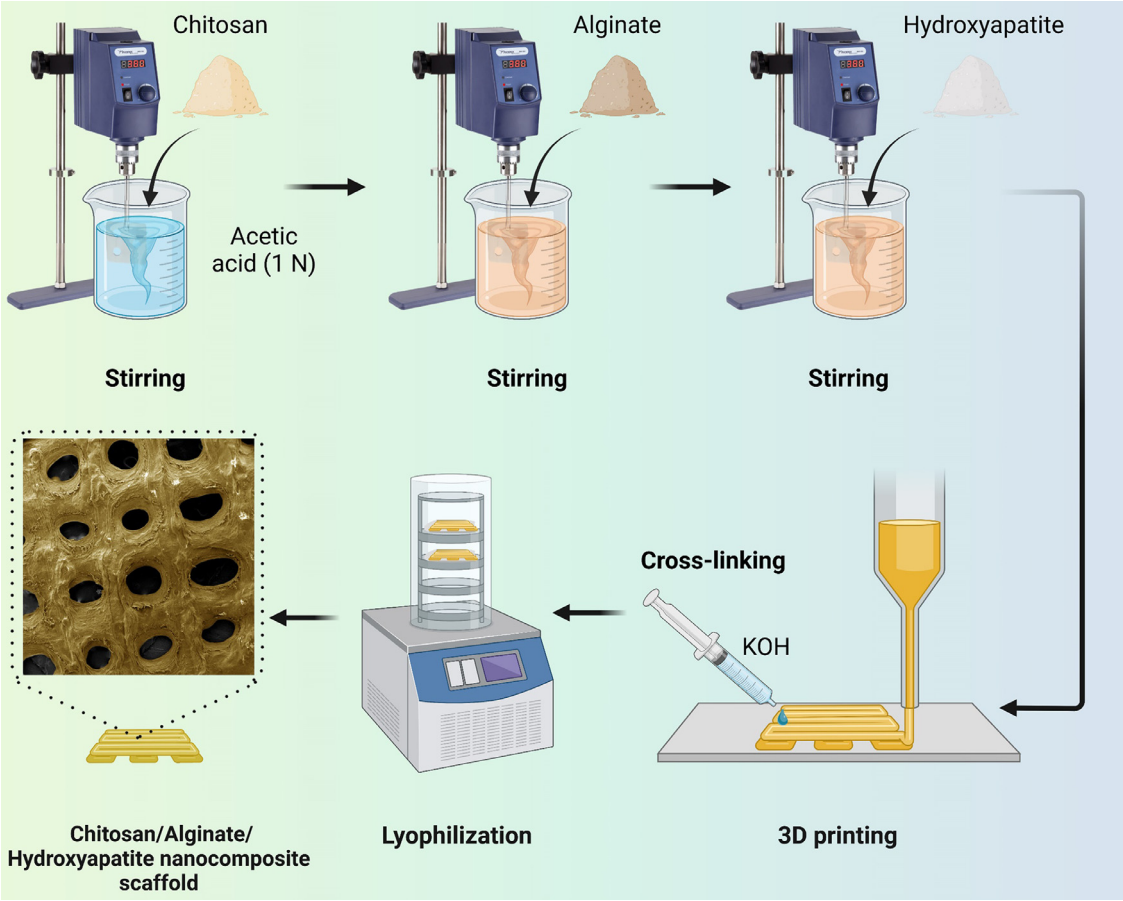

Fig. 1. Schematic illustration of the preparation and 3D printing of the nanocomposite scaffolds.

is considered a double-edged sword; by decreasing pore size, the available surface area increases; on the other hand, a pore size less than a proper size hardens cell migration to the scaffolds. Hence, the scaffold microstructure should be precisely tailored to be compatible with specific cells and tissues [6,7].

Polymers are extensively investigated for bone tissue engineering; especially natural polymers have notably drawn attention due to their biocompatibility and biodegradability [8–10]. Chitosan is a cationic polysaccharide that demonstrates excellent characteristics namely biocompatibility, non-toxicity, biodegradability, antimicrobial characteristics, and availability [11–13]; chitosan scaffolds enhance cell adhesion, proliferation, and osteoblast differentiation and mineralization [14,15].

Various methods can be employed to fabricate porous bone tissue engineering scaffolds, namely freeze drying, gas foaming, solvent casting, and thermally-induced phase separation. However, the size, shape, and interconnectivity of pores cannot be precisely controlled using these conventional methods. Furthermore, the majority of these methods make it challenging to produce scaffolds with customized porosity for certain defects. Additive manufacturing methods, such as extrusion-based printing, have the potential to design and develop a complex architecture for scaffolds using computer-aided design (CAD) files and computer-aided manufacturing (CAM) by 3D printers [16–18].

Despite the favorable characteristics of chitosan for bone tissue engineering, its poor printability has limited its potential for further applications. In this study, we developed a chitosan-based hydrogel blended with alginate and hydroxyapatite to increase the printability of the hydrogel. The hydrogel was printed with the extrusion-based printing method without increasing the temperature of the polymer. Afterward, the physicochemical characteristics of the printed scaffolds and their *in vitro* bioactivity and biocompatibility were investigated.

2. Materials and methods

2.1. Three-dimensional (3D) printing of scaffolds

Chitosan (Sigma-Aldrich, USA) was dissolved in an acetic acid (Merck, Germany) solution (1% v/v) with a concentration of 4.5% w/v at room temperature under mechanical stirring for 3 h. Then, alginate (Sigma-Aldrich, USA) with a concentration of 0.45% w/v was added to the chitosan solution and mechanically stirred for 1 h. Afterward, hydroxyapatite (Sigma-Aldrich, USA) was added to the chitosan and alginate solution at different ratios (2.5, 5, and 10% of the chitosan and alginate dry weights) and stirred for 1 h to produce Chit/Alg, Chit/Alg/2.5HA, Chit/Alg/5HA, and Chit/Alg/10HA hydrogels, respectively. The scaffolds were designed using CATIA v.5 software (Dassault Systèmes,Vélizy-Villacoublay, France); briefly, 20 mm × 20 mm × 2 mm mesh scaffolds were designed and printed using Abtin II (Abtinteb Fanavar, Iran) 3D printer. Upon printing, KOH (Merck, Germany) was added dropwise to the printed scaffold, and after 10 min, the scaffolds were collected and moved to -20 °C. The scaffolds were then lyophilized using an Alpha 1-2 LD plus freeze dryer (Christ, Germany) for 24 h at 50 °C and 0.040 bar (**Fig. 1**).

2.2. 3D printed scaffolds characterization

Attenuated Total Reflectance Fourier Transform Infrared Spectroscopy (ATR-FTIR, Bruker, Germany) was used to determine the functional groups present in the fabricated scaffolds. Detailed information regarding morphological and elemental characteristics of the printed scaffolds were examined using scanning electron microscopy (SEM, TES-

CAN VEGA3 XMU, Tescan, Brno, Czech Republic) paired with energy dispersive X-ray spectroscopy (EDS).

2.3. Porosity and pore size measurement

The porosity, pore size distribution, and average pore size of the printed scaffolds were assessed via evaluating SEM images by the Image J software (NIH, USA). The surface area of pores was divided by the overall picture area to calculate porosity. Additionally, several scanning electron microscopy (SEM) pictures were measured, and the averages were calculated.

2.4. Scaffolds swelling behavior

According to a methodology previously described, the behavior of the printed scaffolds swelling was measured. The 10 mm × 10 mm × 2 mm mesh scaffolds measuring were initially weighed dry before being soaking in phosphate-buffered saline (PBS) and incubated at 37 ˚C. Following the removal of the surplus water from the scaffolds, the samples' wet weight was measured at set time intervals. The following formula was used to calculate the scaffold swelling ratio: swelling ratio = Ww - Wd / Wd, where Ww represents the weight of the wet sample and Wd represents the original dry weight of the same sample.

2.5. Scaffolds bioactivity

The bioactivity of the scaffold samples was evaluated *in vitro* by immersing them in the simulated body fluid (SBF-1X). In the first step, portions of the scaffolds with consistent dimensions were obtained, and the requisite volume of SBF for the scaffold soaking was determined using the formula V = S/10, where V is the required volume in ml and S is the surface area of the scaffolds in mm. After 28 days, the scaffolds were withdrawn from SBF, washed using SBF and lyophilized. Finally, the scaffolds were investigated using SEM.

2.6. Mesenchymal stem cells (MSCs) isolation and characterization

The ethical standards for using laboratory animals were followed for all animal operations, which have been approved by the ethical committee of the Hamadan University of Medical Sciences (IR.UMSHA.REC.1400.941). The femur and tibia of a healthy Wistar rat that was 3–4 weeks old and weighed 100–120 g were isolated under sterile conditions after being ethically sacrificed while receiving deep anesthesia (75 mg of ketamine and 5 mg of xylazine/kg). The samples were immersed in low glucose DMEM (L-DMEM) containing 2% penicillin/streptomycin. Without first separating the epiphysis, the diaphysis was cut in half by removing the joint capsules from each end of the bone. The bone marrow cavity was repeatedly washed, and the cells were collected in a sterile petri dish using a disposable aseptic syringe and L-DMEM medium supplemented with antibiotics. The obtained suspension was filtered through a 200-mesh sieve and then centrifuged for 10 min at 2000 rpm. The supernatant was withdrawn, and cells were resuspended in a medium containing 10% FBS and 1% penicillin and streptomycin antibiotics and moved into a culture flask, and incubated at 37 ˚C with 5% CO_2. One flask was used to cultivate cells obtained from one rat. Non-adherent cells were removed from the medium by replacing it with a DMEM medium containing 10% FBS and 1% penicillin after two days. Cells were passaged using 0.25% Trypsin/EDTA once they had reached 90% confluency. After three passages, cells were collected for the flow cytometric analysis of cell surface markers, including CD34, CD44, and CD90.

2.7. Cell proliferation analysis

Cell Counting Kit-8 (CCK-8) assay was used to measure the viability of cells on the various scaffolds (n = 3 for each group). Rat bone marrow Mesenchymal stem cells (MSCs) were grown at 37 ˚C in 5% CO_2 in the DMEM medium with 10% fetal bovine serum and 1% penicillin/streptomycin antibiotic. The scaffolds with a thickness of 2 mm, a size of 5 mm, and a weight of approximately 2.4 mg were sterilized with 70% ethanol and exposed to UV irradiation for 2 h, and then were rinsed two times using PBS and culture media. The specimens were put in a 96-well plate, and the MSCs were seeded on the top of each scaffold at a density of 5×10^3 cells per scaffold.

The scaffolds were transferred to new wells after being cultured for 24 and 72 h (the number of cells was counted as they grew on the scaffolds rather than the plate), and 10 μL of the CCK-8 solution was added to each well. After 4 h, 100 μL of each sample was moved into a 96-well plate and measured by a microplate spectrophotometer at a wavelength of 450 nm [19].

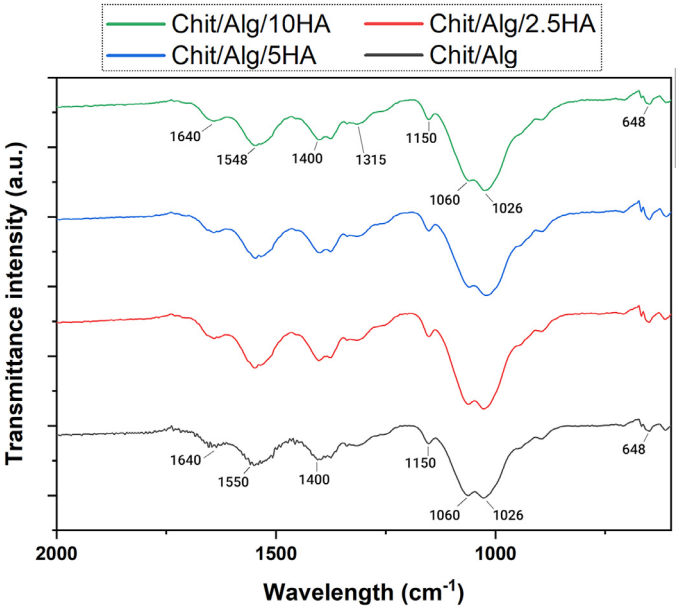

Fig. 2. ATR-FTIR spectra of the Chit/Alg, Chit/Alg/2.5HA, Chit/Alg/5HA, and Chit/Alg/10HA scaffolds.

2.8. Statistical analysis

Data were reported as mean ± standard deviation (Mean ± SD) and were analyzed using GraphPad Prism v.9 (San Diego, CA, US) and Origin Pro v.9 (Northampton, MA, US). The one-way analysis of variance (ANOVA) and post hoc Tukey's tests was used to analyze statistical data. For all of the tests, a p-value less than 0.05 was regarded as statistically significant.

3. Results and discussion

3.1. Structural characterization of the fabricated composite scaffolds

3.1.1. ATR-FTIR

Fig. 2 shows the ATR-FTIR spectra of the fabricated samples. The peak at 1640 cm^{-1} corresponds to the stretching vibrations of C=O in the sodium alginate and amide in the chitosan. The asymmetric adsorption band at 1400 cm^{-1} appears in response to oscillations of the COO- groups and indicates the presence of carboxyl groups in alginate molecules. Bands at 1550 and 1150 cm^{-1} refer to oscillations of the NH bond and indicate the presence of amine groups in chitosan. The bands at 1026 and 1060 cm^{-1} correspond to C-O stretching. The bond at 1315 cm^{-1} is also related to the CH_2 vibrations [20]. Also, after HA incorporation, no significant change was observed in the band at 1040 cm^{-1} ($PO_4{}^3$), attributed to a probable overlap with other bands.

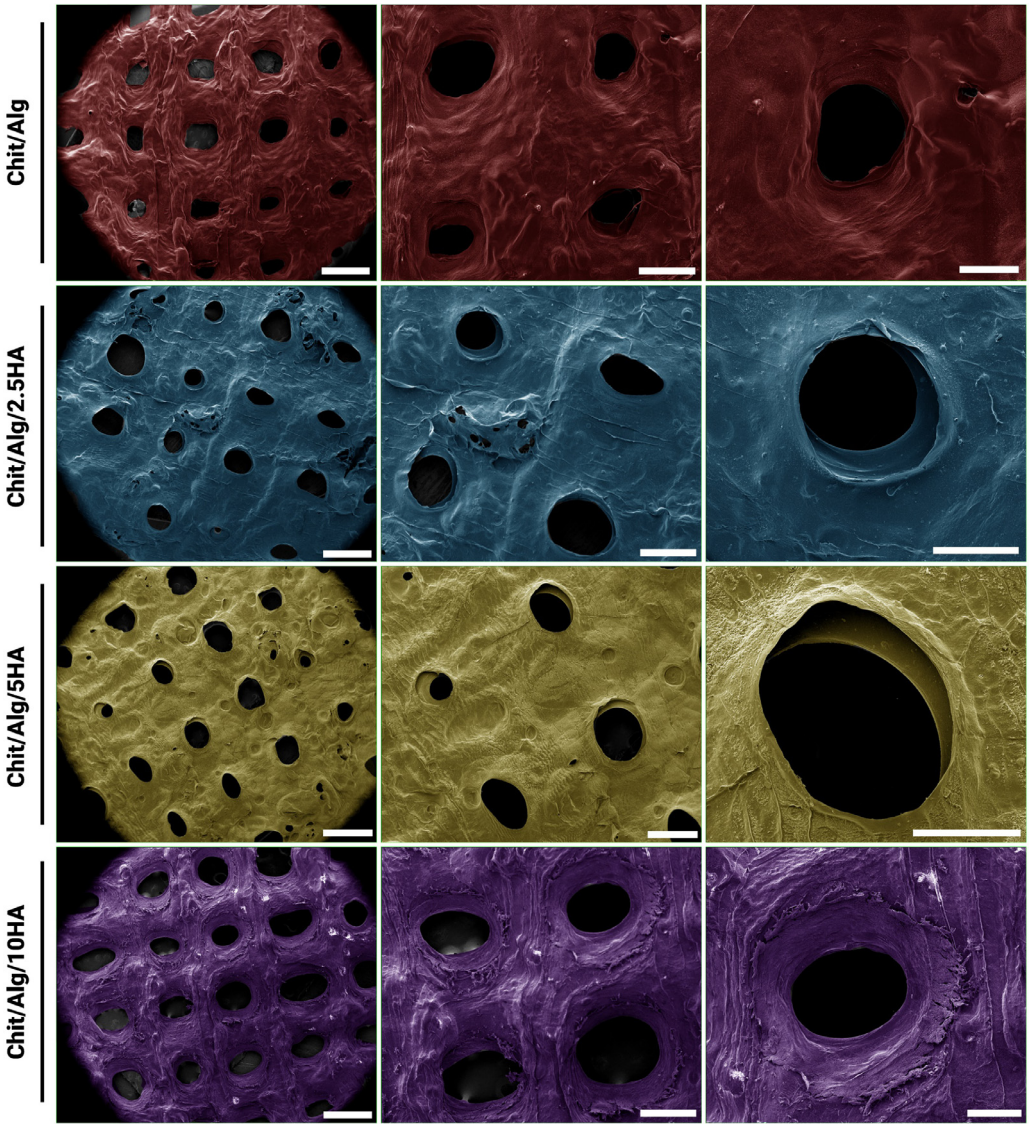

Fig. 3. Representative SEM images of the Chit/Alg, Chit/Alg/2.5HA, Chit/Alg/5HA, and Chit/Alg/10HA scaffolds. Scale bars from left to right represent 1 mm, 500 μm, and 250 μm.

3.1.2. SEM and EDS

Hydrogels with varying amounts of HA were prepared using the blending technique. The extrusion-based 3D printing technique successfully produced scaffolds of the same size and thickness. The hydrogel possessed a degree of elasticity and fluidity. After the printing process, a 20 mm × 20 mm × 2 mm scaffold was developed with different pores sizes. Through SEM (Fig. 3), it is observed that the scaffolds demonstrate a porous structure with clearly defined pores of a thick pore wall structure. Due to the lyophilization process, no shrinkage or other textural abnormalities were observed.

The energy dispersive spectrum (EDS) mapping images show that both Ca and P elements are distributed evenly in the whole scaffolds, indicating the homogenous distribution of HA in the printed scaffolds (Fig. 4). Al element in (Fig. 4A) is related to the background due to the SEM sample holder.

3.2. Porosity and pore size of the scaffolds

As shown in Fig. 5**A,** the Chit/Alg and Chit/Alg/10HA scaffolds show more uniformly distributed and oriented porous structures. The porosity of the printed Chit/Alg, Chit/Alg/2.5HA, Chit/Alg/5HA, and Chit/Alg/10HA scaffolds was measured to be 9.53 (± 1.28) %, 10.31 (± 0.71) %, 10.41 (± 0.68) %, and 16.62 (± 0.61) %, respectively (Fig. 5**B**). The pore size of the Chit/Alg, Chit/Alg/2.5HA, Chit/Alg/5HA, and Chit/Alg/10HA scaffolds ranged from 89-331, 118-289, 40-280, and 190-464 μm, respectively. Furthermore, the average pore size of the Chit/Alg, Chit/Alg/2.5HA, Chit/Alg/5HA, and Chit/Alg/10HA scaffolds were 176.5, 206.9, 169.4, and 285.5 μm, respectively (Fig. 5**C**).

The pore size has been demonstrated to significantly influence the generation of new bone and associated regeneration processes, such as angiogenesis and bone tissue ingrowth. In brief, the minimum acceptable pore size for bone tissue engineering scaffolds is 100 μm. Smaller pores are inappropriate for adequate nutrients and oxygen transport to maintain cell viability and preserve primary cellular activities. Additionally, it has been proposed that for the optimal osteogenesis and vascularization, interconnected pore sizes should be maintained in the range of 200–350 μm [21–23].

Cortical or compact bone is typically 10–30% porous, whereas cancellous bone has a porosity of 30–90% in nature. Higher levels of bone porosity are associated with lower bone density and a greater propen-

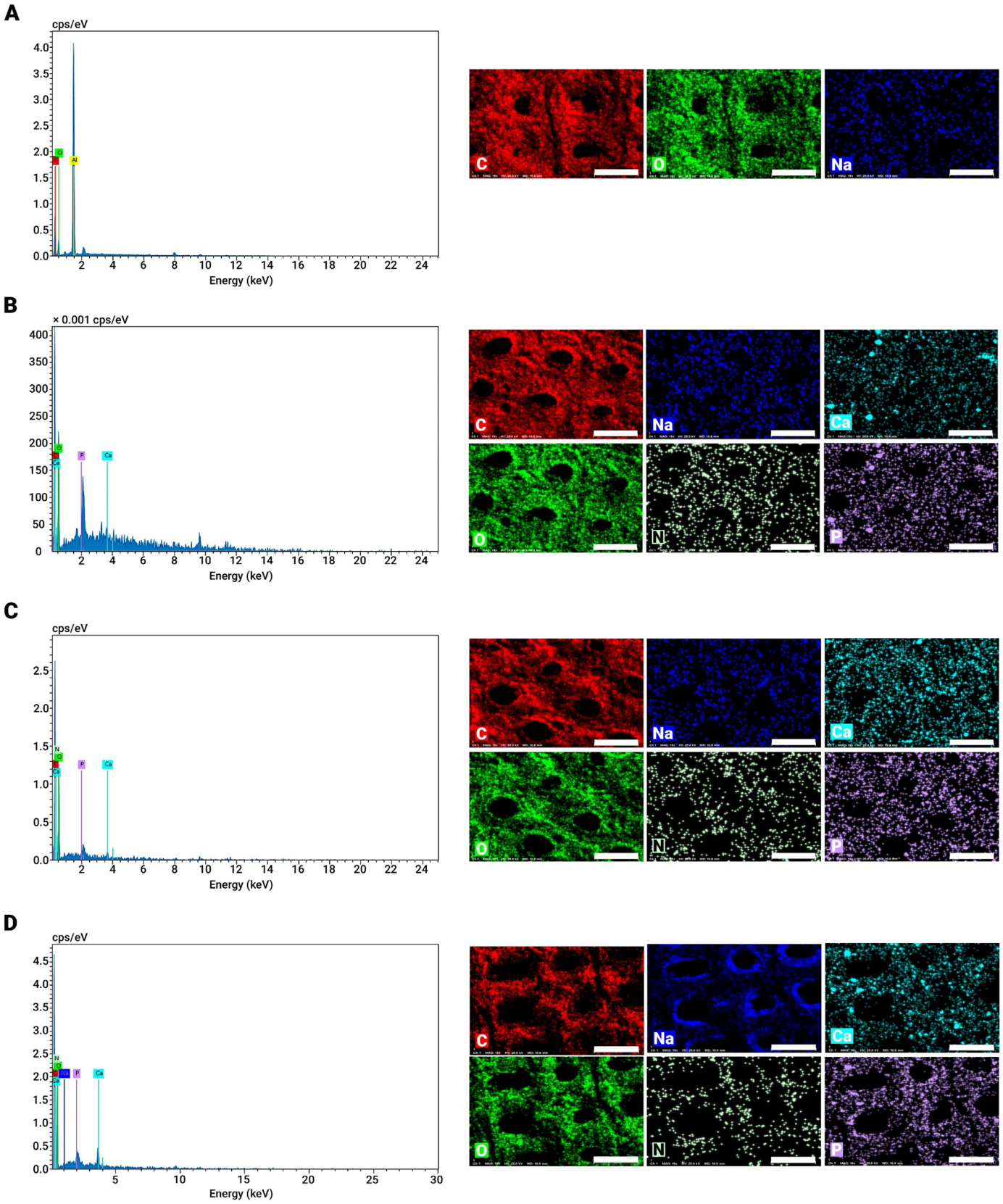

Fig. 4. EDS analyses of the printed **(A)** Chit/Alg, **(B)** Chit/Alg/2.5HA, **(C)** Chit/Alg/5HA, and **(D)** Chit/Alg/10HA scaffolds (white scale bars indicate 2 mm).

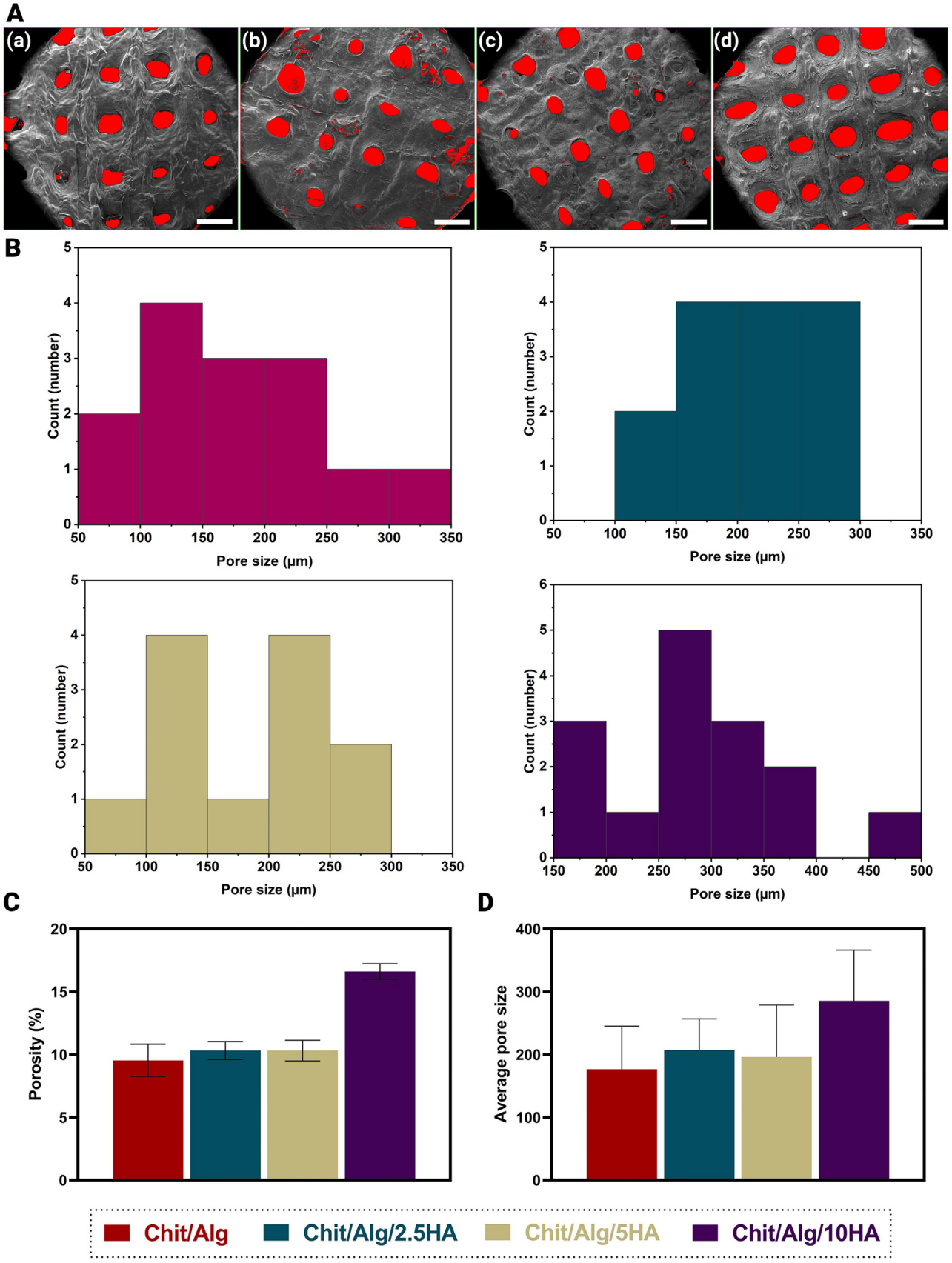

Fig. 5. **(A)** Corresponding SEM images of the printed (a) Chit/Alg, (b) Chit/Alg/2.5HA, (c) Chit/Alg/5HA, and (d) Chit/Alg/10HA scaffolds indicating their pores (white scale bars indicate 1 mm). **(B)** Pore size distribution of the printed scaffolds. **(C)** and **(D)** bar graphs showing the porosity and average pore size of the printed scaffolds, respectively.

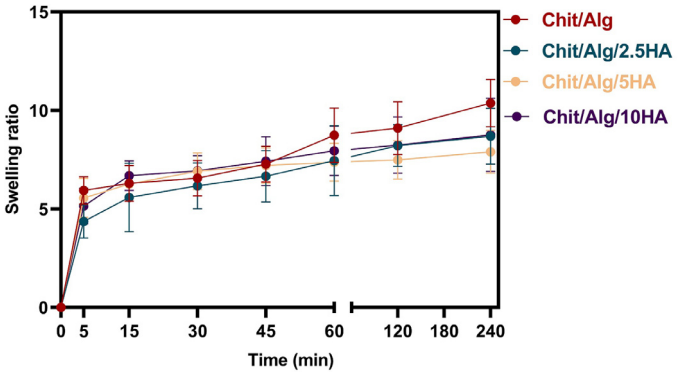

Fig. 6. The swelling ratio of the Chit/Alg, Chit/Alg/2.5HA, Chit/Alg/5HA, and Chit/Alg/10HA printed scaffolds.

sity for bone fractures observed in patients bearing osteoporosis [24,25]. Some studies have shown that high porosity is ideal for bone tissue engineering; however, the mechanical stability of scaffolds was decreased by increasing porosity. Thus, a fundamental difficulty in creating bone replacement scaffolds is balancing mechanical strength and porosity [26,27]. The porosity of scaffolds is slightly increased by increasing the HA concentration; however, Chit/Alg/10HA exhibited the highest porosity. Also, the average pore size of the Chit/Alg/10HA scaffold was demonstrated to be larger than the other scaffold groups. It seems that the presence of HA increases the printability of the prepared hydrogel, which results in a higher printing resolution and increased pore size besides more uniformly distributed pores.

3.3. Scaffolds swelling behavior

Regarding the ability of the dry scaffolds to absorb water, all samples exhibit a high swelling capacity (Fig. 6). The increased swelling ratio that results from prolonged soaking implies that the water absorption levels have grown; nevertheless, the growing water absorption rate has

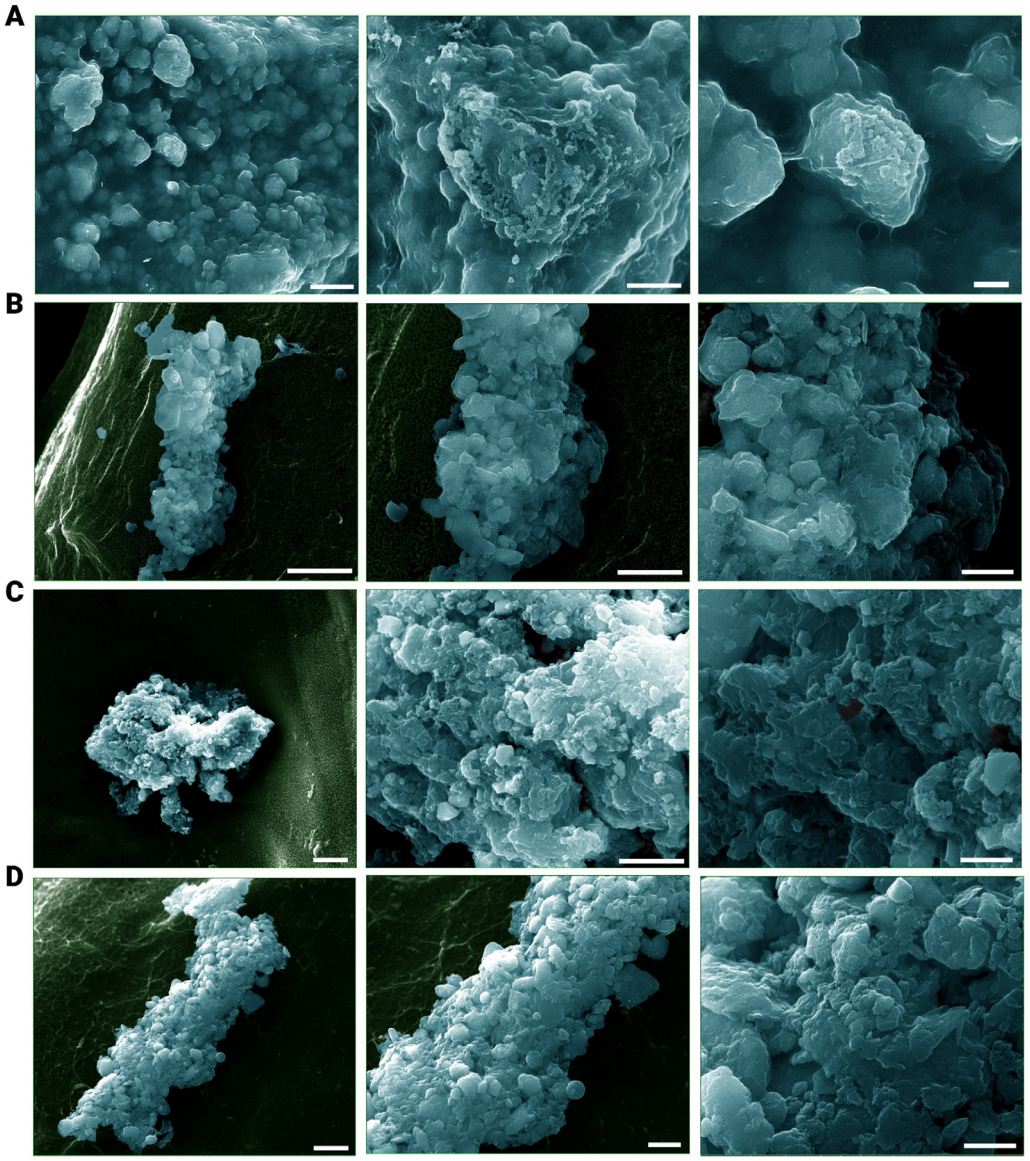

Fig. 7. SEM images of the surface of **(A)** Chit/Alg, **(B)** Chit/Alg/2.5HA, **(C)** Chit/Alg/5HA, and **(D)** Chit/Alg/10HA scaffolds for evaluating apatite formation after 28 days submerging in SBF-1X. Scale bars from left to right represent 10 mm, 5 mm, and 2 mm.

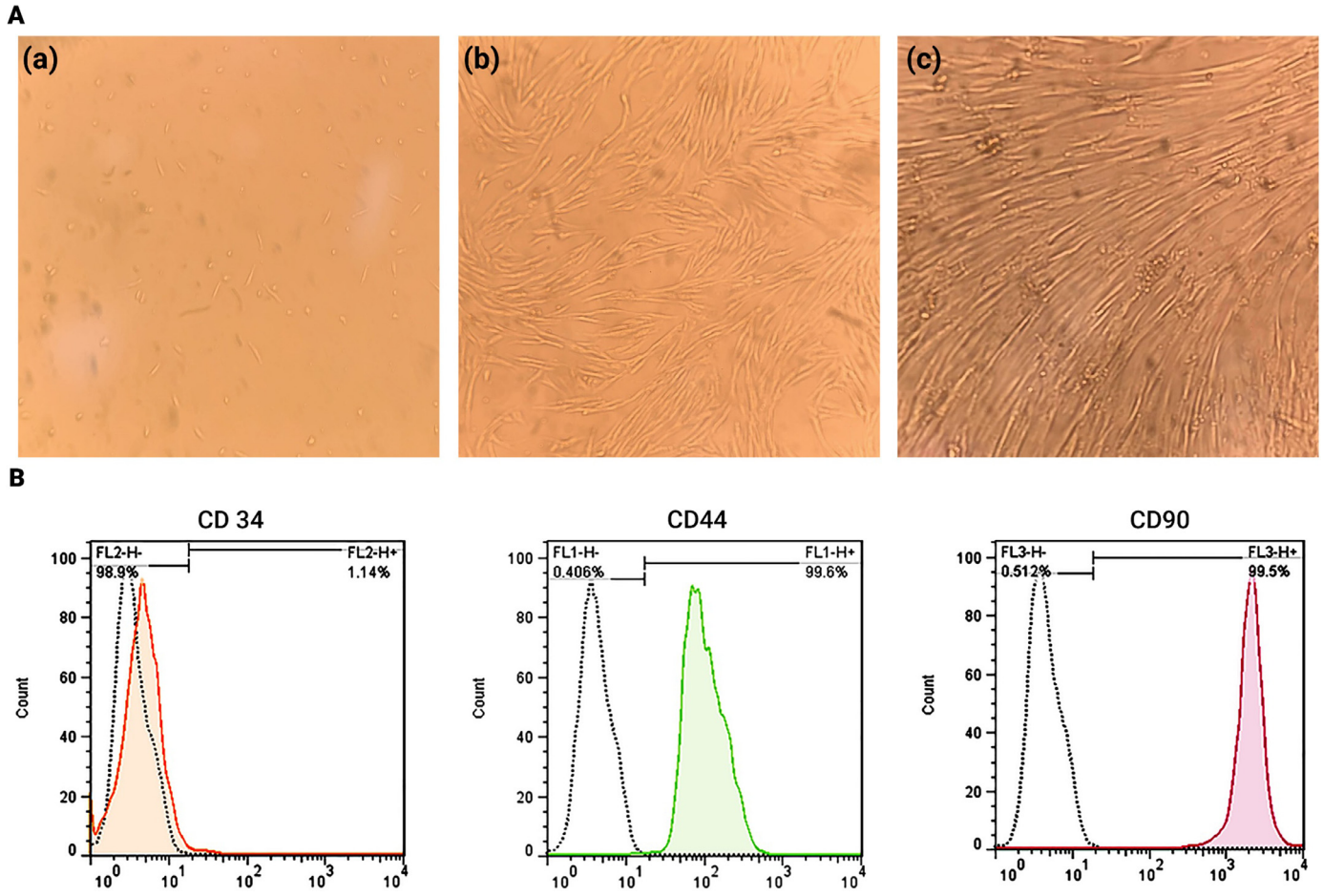

Fig. 8. **(A)** Rat bone marrow mesenchymal stem cells morphology under light microscopy as (a) primary, (b) Passage 3 with about 60% confluency, and (c) Passage 3 with more than 90% confluency. Images were acquired at low magnification (20X). **(B)** The stem cell surface marker analysis using flow cytometry shows CD34 negative surface markers and CD44 and CD90 positive surface markers for the stemness of isolated cells.

reduced, and the scaffolds achieved a swelling equilibrium. The Chit/Alg scaffold possesses the highest swelling ratio; however, the difference was not statistically significant. In addition, the results show that the hydroxyapatite incorporation does not affect the scaffolds swelling kinetics, as all scaffolds swelled after submerging in the PBS.

The transmittance of biological fluids, nutrient absorption, and cellular waste transportation through biomaterials are all essential to the success of tissue engineering procedures, making water absorption capacity a crucial property of tissue engineering scaffolds [28]. A high swelling ratio in the manufactured scaffolds is necessary to preserve the aforementioned features. In addition, The pH of the surrounding fluid has a significant impact on the expansion behavior. Due to the biological applications of the scaffolds, their swelling behavior was tested in phosphate-buffered saline (pH 7.4). Utilizing such a method makes it possible to assess how the scaffolds behave after they have been implanted within the body [29,30].

3.4. Scaffolds bioactivity

All of the scaffolds show apatite formation upon incubation in SBF. The size of the apatite particles formed on the Chit/Alg scaffold is larger than that of the particles on the HA-containing scaffolds. Furthermore, the number of formed apatite particles increases with the increase in the hydroxyapatite content of the scaffolds **(Fig. 7)**.

SBF is a supersaturated solution of metastable calcium phosphate with regard to apatite. It has been indicated that since there is a significant barrier to the homogeneous nucleation of apatite from SBF, external stimulation is required to initiate the heterogeneous nucleation of apatite. Numerous nano-HA particles potentially serving as nucleation sites were present on the Chit/Alg/HA composite scaffolds. Thus, the composite scaffolds were more able to support the formation of apatite compared to the chitosan/alginate scaffolds. For this reason, the Chit/Alg/HA composite scaffolds attained a higher apatite deposition than Chit/Alg throughout the same period. The number of generated nuclei impacted the amount of minerals that could accumulate on each nucleus since the local mineralization microenvironment has a limited level of inorganic ions. As a result, the particles generated on the composite scaffold were smaller than those on the chitosan scaffold **(Fig. 7)** [31].

According to the studies, adding components with the capability to interact with or bind to biological tissues has been shown to promote bioactivity. Enhanced scaffold bioactivity has the potential to enhance osteoconduction (bone tissue ingrowth), osteointegration (stable attachment of the scaffolds to host bone tissue), osteoinduction (causes immature cells to differentiate into osteogenic cells), and angiogenesis (increases blood vessel growth) [32–35].

3.5. Bone marrow mesenchymal stem cells (MSCs) characterization

Stem cells with enhanced regeneration ability have the potential to self-renew and specialize into a wide variety of cell types, resulting in superior tissue regeneration [36,37]. In order to characterize isolated

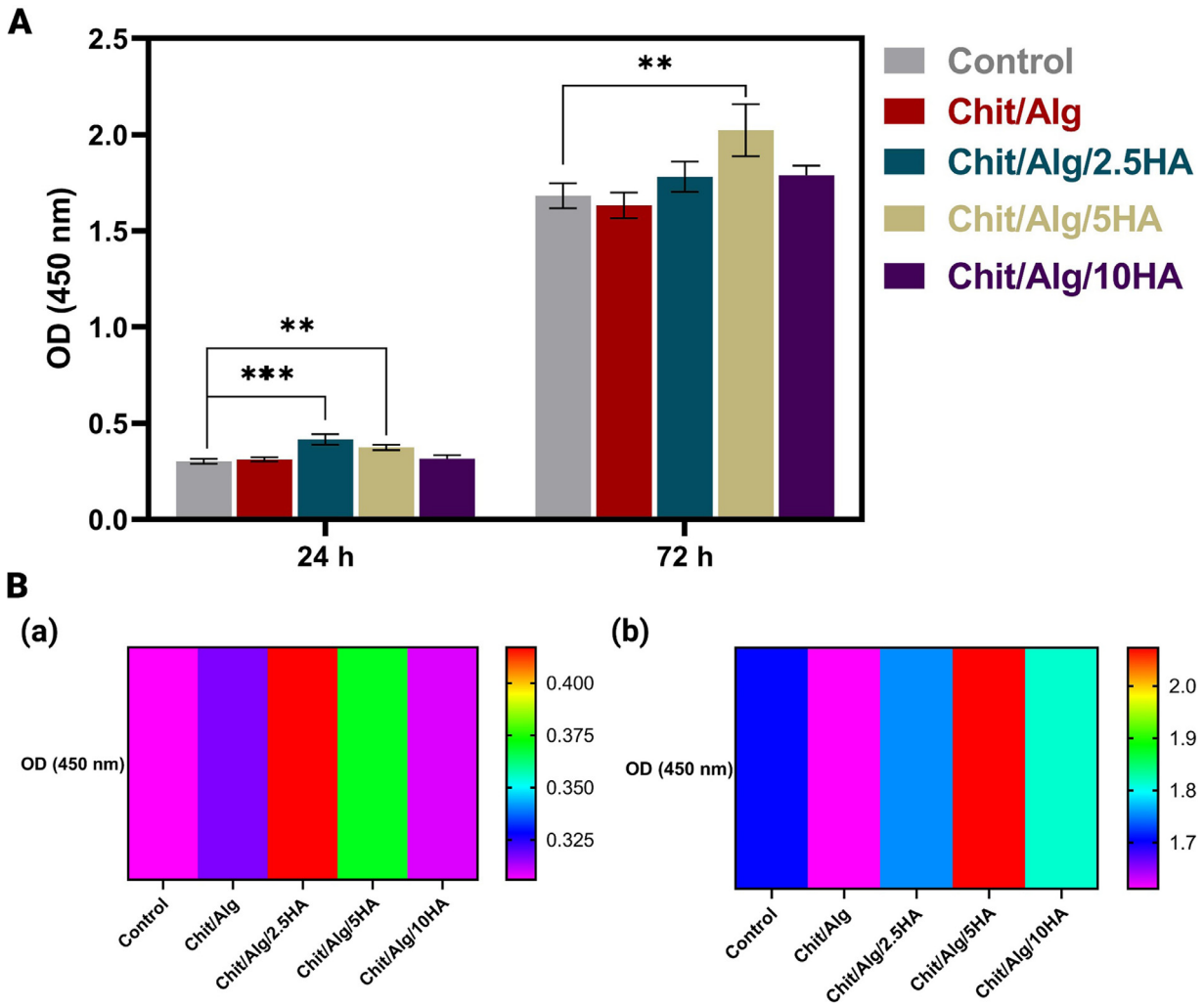

Fig. 9. **(A)** Cell viability of rat bone marrow MSCs cultured on the printed Chit/Alg, Chit/Alg/2.5HA, Chit/Alg/5HA, and Chit/Alg/10HA scaffolds in comparison with two-dimensional cultured cells (control) after 24 h and 72 h. **(B)** Corresponding heatmap of the viability of the cells after (a) 24 h and (b) 72 h. (**: $p < 0.01$, ***: $p < 0.001$).

MSCs, a morphological analysis was performed (**Fig. 8A**), and flow cytometry was used to quantify the surface marker expression. The high purity of isolated MSCs is demonstrated by the high level of positive surface markers (CD44, CD90) expression and the low level of negative surface markers (CD34) expression (**Fig. 8B**).

3.6. Cell proliferation analysis

CCK-8 assay was conducted using rat bone marrow MSCs on the different scaffold samples to investigate the cytocompatibility of the printed scaffolds. The optical microscope investigation showed that MSCs incubated with the scaffolds showed normal morphology and proliferation (**Fig. S1**). After 24 h, all of the scaffold samples showed increased cell viability compared to the control; however, only the Chit/Alg/2.5HA and Chit/Alg/5HA samples showed a statistically significant increase in viability. After 72 h, the Chit/Alg/HA composite scaffolds demonstrated increased cell viability, in which the Chit/Alg/5HA scaffold sample showed a statistically significant increase compared to the control group (**Fig. 9**).

Materials implanted in hosts should be biologically inert and enable tissue development. In addition to their physicochemical characteristics, scaffolds also need to be biologically compatible. Biocompatibility is a key criterion for all bone scaffolds and has been defined in a variety of ways. The capacity of a scaffold to sustain normal cellular function, including molecular signaling, without causing any immediate or long-term adverse consequences on the host tissue is known as biocompatibility [79]. Ideal bone scaffolds are osteoconductive scaffolds that promote bone cell adhesion, proliferation, and extracellular matrix formation on their surface and pores [24,38].

The compositions of the scaffolds are generally regarded as one of the most critical factors that influence biocompatibility and cytotoxicity characteristics. Chitosan and alginate have received FDA approval to be used as biomaterials; In addition, nanohydroxyapatite has been indicated to have noncytotoxic and genotoxic profiles. Hence, the biocompatibility of chitosan, alginate, and hydroxyapatite as the components of the scaffold is represented in the cytotoxicity results [39–41].

Potential clinical applications of the printed scaffolds are shown in **Fig. 10**. Complex bone defects in the craniofacial area can be filled with 3D printed scaffolds to accelerate bone regeneration. Due to the complex structure of craniofacial bones, defects in this area cannot be regenerated by scaffolds fabricated by conventional methods. The printed scaffold architecture can be adjusted based on the defect and patient to provide the optimal treatment for the patients [42–44].

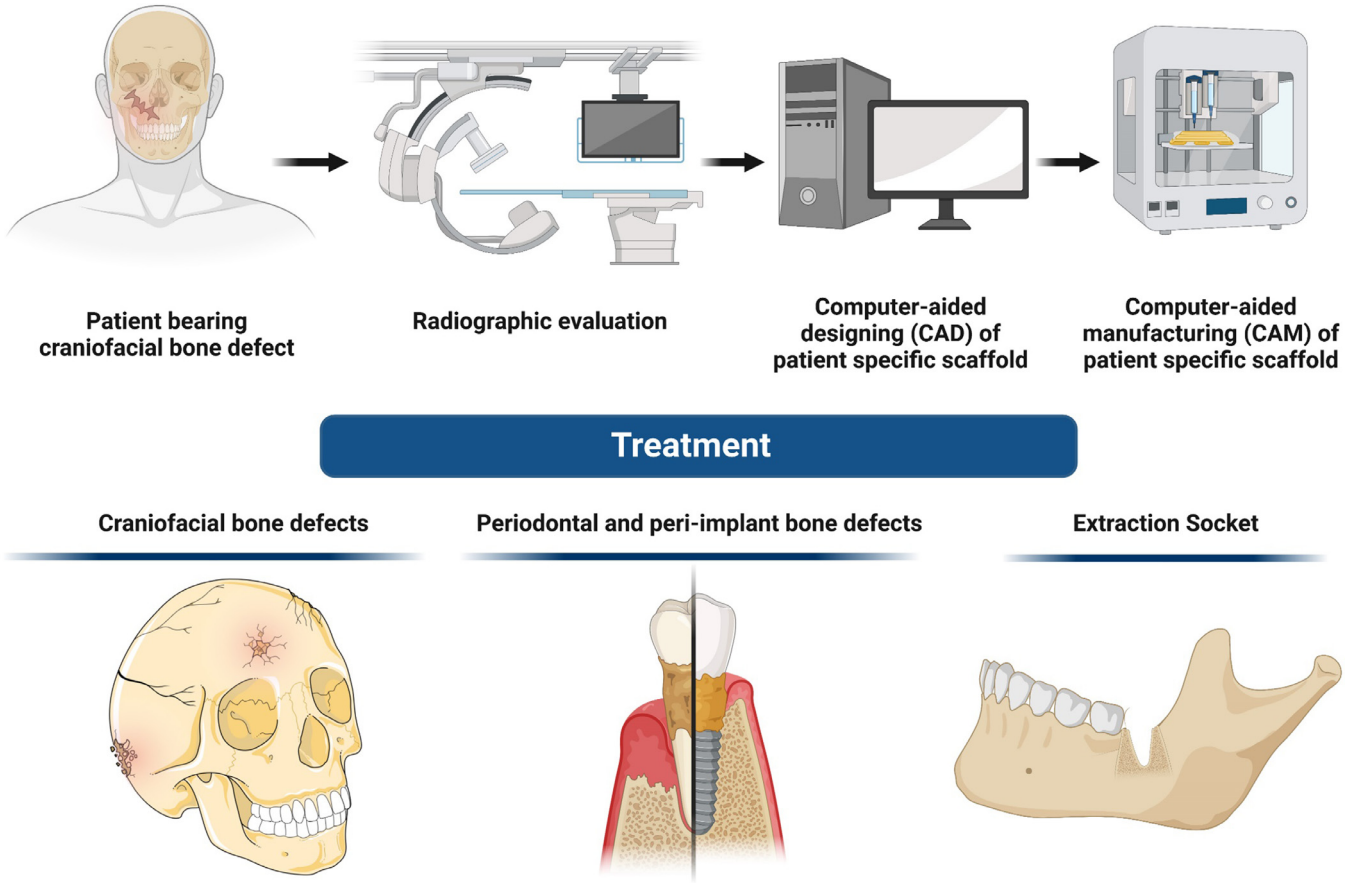

Fig. 10. Schematic illustration of potential applications of patient-specific scaffolds developed by CAD/CAM systems.

4. Conclusion

In the present study, we successfully developed a printable chitosan-based hydrogel partially substituted with alginate and hydroxyapatite. All of the printed nanocomposites with the different hydroxyapatite concentrations (2.5, 5, and 10%) showed a homogenous distribution of hydroxyapatite in their polymeric matrix. The addition of hydroxyapatite increased porosity and average pore size in the Chit/Alg/5HA scaffold. Furthermore, the HA addition increased apatite formation amounts and decreased the size of apatite crystals. All of the scaffold samples showed biocompatible properties and did not have toxicity toward mesenchymal stem cells compared to the control group. Furthermore, the scaffolds containing 5% hydroxyapatite showed a significant increase in cell viability in comparison with the control. Overall, printed Chit/Alg/HA nanocomposite scaffolds desinged with desired characteristics could be considered as a promising option for craniofacial complex bone defects regeneration after further *in vitro* and *in vivo* evaluations regarding their osteogenic differentiation potential.

Declaration of Competing Interest

The authors declare that they have no known competing financial interests or personal relationships that could have appeared to influence the work reported in this paper.

CRediT authorship contribution statement

Satar Yousefiasl: Conceptualization, Data curation, Formal analysis, Investigation, Methodology, Software, Visualization, Writing – original draft, Writing – review & editing. **Esmaeel Sharifi:** Conceptualization, Methodology, Supervision, Validation, Writing – review & editing. **Erfan Salahinejad:** Conceptualization, Methodology, Software, Writing – review & editing. **Pooyan Makvandi:** Software, Visualization, Validation, Writing – review & editing. **Soussan Irani:** Conceptualization, Project administration, Supervision, Validation, Writing – review & editing.

Acknowledgments

The study was funded by Vice-chancellor for Research and Technology, Hamadan University of Medical Sciences.

Supplementary materials

Supplementary material associated with this article can be found, in the online version, at doi:10.1016/j.engreg.2022.09.005.

References

[1] Y. Lin, S. Huang, R. Zou, X. Gao, J. Ruan, M.D. Weir, M.A. Reynolds, W. Qin, X. Chang, H. Fu, H.H.K. Xu, Calcium phosphate cement scaffold with stem cell co–culture and prevascularization for dental and craniofacial bone tissue engineering, Dent. Mater. (2019).
[2] L. Larsson, A.M. Decker, L. Nibali, S.P. Pilipchuk, T. Berglundh, W.V Giannobile, Regenerative medicine for periodontal and peri-implant diseases, J. Dent. Res. 95 (3) (2015) 255–266.
[3] A. Saltz, U. Kandalam, Mesenchymal stem cells and alginate microcarriers for craniofacial bone tissue engineering: a review, J. Biomed. Mater. Res. Part A (2016).
[4] E. Sharifi, S.A. Sadati, S. Yousefiasl, R. Sartorius, M. Zafari, L. Rezakhani, M. Alizadeh, E. Nazarzadeh Zare, S. Omidghaemi, F. Ghanavatinejad, M. Jami, E. Salahinejad, H. Samadian, A.C. Paiva-Santos, P. De Berardinis, A. Shafiee, F.R. Tay, S. Pourmotabed, P. Makvandi, Cell loaded hydrogel containing Ag-doped bioactive glass–ceramic nanoparticles as skin substitute: antibacterial properties, immune response, and scarless cutaneous wound regeneration, Bioeng. Transl. Med. (2022).

[5] T. Kuang, S. Chen, Z. Gu, Z. Shen, A. Hejna, M.R. Saeb, F. Chen, M. Zhong, T. Liu, A facile approach to fabricate load-bearing porous polymer scaffolds for bone tissue engineering, Adv. Compos. Hybrid Mater. (2022) 1–9.
[6] L. Roseti, V. Parisi, M. Petretta, C. Cavallo, G. Desando, I. Bartolotti, B. Grigolo, Scaffolds for bone tissue engineering: state of the art and new perspectives, Mater. Sci. Eng. C 78 (2017) 1246–1262.
[7] F. Rey, B. Barzaghini, A. Nardini, M. Bordoni, G.V. Zuccotti, C. Cereda, M.T. Raimondi, S. Carelli, Advances in tissue engineering and innovative fabrication techniques for 3-D-structures: translational applications in neurodegenerative diseases, Cells 9 (7) (2020) 1636.
[8] F. Zhang, M. Lian, A. Alhadhrami, M. Huang, B. Li, G.A.M. Mersal, M.M. Ibrahim, M. Xu, Laccase immobilized on functionalized cellulose nanofiber/alginate composite hydrogel for efficient bisphenol A degradation from polluted water, Adv. Compos. Hybrid Mater. (2022) 1–13.
[9] H. Manoochehri, M. Ghorbani, M.M. Moghaddam, M.R. Nourani, P. Makvandi, E. Sharifi, C. Authors, Strontium doped bioglass incorporated hydrogel-based nanocomposite scaffold for amplified bone tissue regeneration, (2022) 1–37.
[10] N. Movagharnezhad, S. Ehsanimehr, P. Najafi Moghadam, Synthesis of poly (N-vinylpyrrolidone)-grafted-magnetite bromoacetylated cellulose via ATRP for drug delivery, Mater. Chem. Horiz. 1 (2) (2022) 89–98.
[11] J. Ni, X. Huang, Y. Bai, B. Zhao, Y. Han, S. Han, T. Xu, C. Si, C. Zhang, Resistance to aggregation-caused quenching: chitosan-based solid carbon dots for white light-emitting diode and 3D printing, Adv. Compos. Hybrid Mater. (2022) 1–11.
[12] M. Zafari, M. Mansouri, S. Omidghaemi, A. Yazdani, S. Pourmotabed, A. Hasanpour Dehkordi, H. Nosrati, M. Validi, E. Sharifi, Physical and biological properties of blend-electrospun polycaprolactone/chitosan-based wound dressings loaded with N-decyl-N, N -dimethyl-1-decanaminium chloride: An in vitro and in vivo study, J. Biomed. Mater. Res. Part B Appl. Biomater. 108 (8) (2020) 3084–3098.
[13] G. Heidari, M. Hassanpour, F. Nejaddehbashi, M.R. Sarfjoo, S. Yousefiasl, E. Sharifi, A. Bigham, T. Agarwal, A. Borzacchiello, E. Lagreca, C. Di Natale, N. Nikfarjam, Y. Vasseghian, Biosynthesized nanomaterials with antioxidant and antimicrobial properties, Mater. Chem. Horiz. 1 (1) (2022) 35–48.
[14] J. Venkatesan, S.K. Kim, Chitosan composites for bone tissue engineering—an overview, Mar. Drugs 8 (8) (2010) 2252–2266.
[15] A. Aguilar, N. Zein, E. Harmouch, B. Hafdi, F. Bornert, D. Offner, F. Clauss, F. Fioretti, O. Huck, N. Benkirane-Jessel, Application of chitosan in bone and dental engineering, Molecules 24 (16) (2019) 3009.
[16] S. Bose, S. Vahabzadeh, A. Bandyopadhyay, Bone tissue engineering using 3D printing, Mater. Today 16 (12) (2013) 496–504.
[17] B. Thavornyutikarn, N. Chantarapanich, K. Sitthiseripratip, G.A. Thouas, Q. Chen, Bone tissue engineering scaffolding: computer-aided scaffolding techniques, Prog. Biomater. 3 (2) (2014) 61–102.
[18] A. Shokri, K. Ramezani, M.R. Jamalpour, C. Mohammadi, F. Vahdatinia, A.D. Irani, E. Sharifi, R. Haddadi, S. Jamshidi, L.M. Amirabad, S. Tajik, A. Yadegari, L. Tayebi, In vivo efficacy of 3D-printed elastin–gelatin–hyaluronic acid scaffolds for regeneration of nasal septal cartilage defects, J. Biomed. Mater. Res. Part B Appl. Biomater. 110 (3) (2022) 614–624.
[19] S. Rahimipour, E. Salahinejad, E. Sharifi, H. Nosrati, L. Tayebi, Structure, wettability, corrosion and biocompatibility of nitinol treated by alkaline hydrothermal and hydrophobic functionalization for cardiovascular applications, Appl. Surf. Sci. 506 (2020) 144657 November 2019.
[20] S.H. Lim, S.M. Hudson, Synthesis and antimicrobial activity of a water-soluble chitosan derivative with a fiber-reactive group, Carbohydr. Res. 339 (2) (2004) 313–319.
[21] M. Meskinfam, S. Bertoldi, N. Albanese, A. Cerri, M.C. Tanzi, R. Imani, N. Baheiraei, M. Farokhi, S. Fare, Polyurethane foam/nano hydroxyapatite composite as a suitable scaffold for bone tissue regeneration, Mater. Sci. Eng. C 82 (2018) 130–140.
[22] J. Rouwkema, N.C. Rivron, C.A. van Blitterswijk, Vascularization in tissue engineering, Trends Biotechnol. 26 (8) (2008) 434–441.
[23] C.H. Tsai, C.H. Hung, C.N. Kuo, C.Y. Chen, Y.N. Peng, M.Y. Shie, Improved bioactivity of 3D printed porous titanium alloy scaffold with chitosan/magnesium-calcium silicate composite for orthopaedic applications, Materials 12 (2) (2019) 203 (Basel).
[24] S. Bose, M. Roy, A. Bandyopadhyay, Recent advances in bone tissue engineering scaffolds, Trends Biotechnol. 30 (10) (2012) 546–554.
[25] T.D. Rachner, S. Khosla, L.C. Hofbauer, Osteoporosis: now and the future, Lancet 377 (9773) (2011) 1276–1287.
[26] S. Wu, X. Liu, K.W.K. Yeung, C. Liu, X. Yang, Biomimetic porous scaffolds for bone tissue engineering, Mater. Sci. Eng. R Rep. 80 (2014) 1–36.
[27] M. Ebrahimi, Porosity parameters in biomaterial science: definition, impact, and challenges in tissue engineering, Front. Mater. Sci. 15 (3) (2021) 352–373.
[28] M. Liu, L. Dai, H. Shi, S. Xiong, C. Zhou, *In vitro* evaluation of alginate/halloysite nanotube composite scaffolds for tissue engineering, Mater. Sci. Eng. C 49 (2015) 700–712.
[29] S. Grabska-Zielińska, A. Sionkowska, K. Reczyńska, E. Pamuła, Physico-chemical characterization and biological tests of collagen/silk fibroin/chitosan scaffolds cross-linked by dialdehyde starch, Polymers 12 (2) (2020) 372 (Basel).
[30] R.M. Felfel, M.J. Gideon-Adeniyi, K.M. Zakir Hossain, G.A.F. Roberts, D.M. Grant, Structural, mechanical and swelling characteristics of 3D scaffolds from chitosan-agarose blends, Carbohydr. Polym. 204 (2019) 59–67.
[31] L. Kong, Y. Gao, G. Lu, Y. Gong, N. Zhao, X. Zhang, A study on the bioactivity of chitosan/nano-hydroxyapatite composite scaffolds for bone tissue engineering, Eur. Polym. J. 42 (12) (2006) 3171–3179.
[32] S.-S. Kim, M. Sun Park, O. Jeon, C. Yong Choi, B.-S. Kim, Poly(lactide-co-glycolide)/hydroxyapatite composite scaffolds for bone tissue engineering, Biomaterials 27 (8) (2006) 1399–1409.
[33] A.R. Vaccaro, The role of the osteoconductive scaffold in synthetic bone graft, Orthopedics 25 (5) (2002) S571–S578.
[34] T. Albrektsson, C. Johansson, Osteoinduction, osteoconduction and osseointegration, Eur. Spine J. 10 (2) (2001) S96–S101.
[35] G. Turnbull, J. Clarke, F. Picard, P. Riches, L. Jia, F. Han, B. Li, W. Shu, 3D bioactive composite scaffolds for bone tissue engineering, Bioact. Mater. 3 (3) (2018) 278–314.
[36] I. Ferreira-Faria, S. Yousefiasl, A. Macário-Soares, M. Pereira-Silva, D. Peixoto, H. Zafar, F. Raza, H. Faneca, F. Veiga, M.R. Hamblin, Stem cell membrane-coated abiotic nanomaterials for biomedical applications, J. Control. Release Off. J. Control. Release Soc. (2022) S0168–S3659.
[37] H. Lin, J. Sohn, H. Shen, M.T. Langhans, R.S. Tuan, Bone marrow mesenchymal stem cells: aging and tissue engineering applications to enhance bone healing, Biomaterials 203 (2019) 96–110.
[38] D. Algul, H. Sipahi, A. Aydin, F. Kelleci, S. Ozdatli, F.G. Yener, Biocompatibility of biomimetic multilayered alginate–chitosan/β-TCP scaffold for osteochondral tissue, Int. J. Biol. Macromol. 79 (2015) 363–369.
[39] R.M. Kavasi, C.C. Coelho, V. Platania, P.A. Quadros, M. Chatzinikolaidou, In vitro biocompatibility assessment of nano-hydroxyapatite, Nanomaterials 11 (5) (2021) 1152.
[40] S. Yousefiasl, H. Manoochehri, P. Makvandi, S. Afshar, E. Salahinejad, P. Khosraviyan, M. Saidijam, S. Soleimani Asl, E. Sharifi, Chitosan/alginate bionanocomposites adorned with mesoporous silica nanoparticles for bone tissue engineering, J. Nanostruct. Chem. (2022) 1–15.
[41] T.I. Shaheen, A.S. Montaser, S. Li, Effect of cellulose nanocrystals on scaffolds comprising chitosan, alginate and hydroxyapatite for bone tissue engineering, Int. J. Biol. Macromol. 121 (2019) 814–821.
[42] C. Ding, Z. Qiao, W. Jiang, H. Li, J. Wei, G. Zhou, K. Dai, Regeneration of a goat femoral head using a tissue-specific, biphasic scaffold fabricated with CAD/CAM technology, Biomaterials 34 (28) (2013) 6706–6716.
[43] H. Naujokat, J. Rohwedder, A. Gülses, O. Cenk Aktas, J. Wiltfang, Y. Açil, CAD/CAM scaffolds for bone tissue engineering: Investigation of biocompatibility of selective laser melted lightweight titanium, IET Nanobiotechnol. 14 (7) (2020) 584–589.
[44] L. Ciocca, F. De Crescenzio, M. Fantini, R. Scotti, CAD/CAM and rapid prototyped scaffold construction for bone regenerative medicine and surgical transfer of virtual planning: a pilot study, Comput. Med. Imaging Graph. 33 (1) (2009) 58–62.